

# AudioViewer: Learning to Visualize Sounds

Yuchi Zhang, Chunjin Song, Willis Peng, Parmis Mohaghegh, Bastian Wandt, and Helge Rhodin  
University of British Columbia  
Vancouver, Canada

{chunjins, wandt, rhodin}@cs.ubc.ca

## Abstract

*A long-standing goal in the field of sensory substitution is enabling sound perception for deaf people by visualizing audio content. Different from existing models that translate between speech and text or text and images, we target immediate and low-level audio to video translation that applies to generic environment sounds as well as human speech. Since such a substitution is artificial, without labels for supervised learning, our core contribution is to build a mapping from audio to video that learns from unpaired examples via high-level constraints. For speech, we additionally disentangle content (phones) from style (gender and dialect) by mapping them to a common disentangled latent space. Qualitative and quantitative results, including a user study, demonstrate that our unpaired translation approach maintains important audio features in the generated video and that videos of faces and numbers are well suited for visualizing high-dimensional audio features that can be parsed by humans to match and distinguish between sounds, words, and speakers.*

## 1. Introduction

Humans perceive their environment through diverse channels, including vision and hearing. Because impairment in any sense can lead to drastic consequences, various approaches have been proposed to substitute lost senses, going all the way to recently popularized attempts to directly interface with neurons in the brain (e.g., NeuraLink [46]). One of the least intrusive approaches is to substitute audio with video, which is, however, challenging due to their high throughput and different modality.

In this paper, we propose a method to visualize audio with natural images in real-time, forming a live video that characterizes the audio content. It is a digital sign language with its own throughput, abstraction, automation, and readability trade-offs. Figure 1 gives an overview of how short audio segments are sequentially mapped to frames of a live video of transforming figures.

The following approaches for audio-to-video translation

exist. However, each comes with drawbacks that we attempt to overcome with a radically different, much lower-level information encoding. Lip-syncing the facial expressions of a virtual avatar from spoken audio [6, 13, 45, 55, 68, 76] allows deaf people to lip-read spoken texts. However, natural lip motion is a result of speaking and only contains a fraction of the audio content, which we validate in a comparative user study. Speech can also be translated to words with a recognition system [48]. For example, the spoken 'dog' would be translated to the text 'dog'. This is intuitive, but such a translation is still indirect and does not contain any vocal feedback or style differences between male and female speakers [49, 58, 74]. Moreover, environmental sounds that cannot be indicated by a single word or lip motion, such as the echo of a dropped object or the repeating beep of an alarm, are ill-represented by all of these existing techniques.

To overcome these limitations, we design AudioViewer as a low-level mapping—at the level of sounds and phones instead of words—which makes it immediate and could be used by infants before they have an understanding of words and language in general. The difficulty is that there is no canonical association to create paired labels between audio and video<sup>1</sup>, which would be needed for supervised learning.

Our core contribution is to learn a mapping from unpaired examples via constraints that enforce the following four high-level properties. First, it would be natural to maintain the frequency of features, i.e., to map unusual sounds to unusual images. We therefore use unsupervised learning to match more likely features and exploit cycle consistency to learn a joint structure between audio and video modalities. Second, humans are able to perceive complex spatial structures but quick and non-natural (e.g., flickering) temporal changes lead to disruption and tiredness [57]. Hence, we enforce smoothness constraints on the learned mapping. Third, we disentangle factors of variations, to separate styles, such as gender and dialect, from content, individual phones, and sounds. Fourth, humans are good at recognizing patterns and objects that they see in their environment, particularly human faces [1, 7, 28, 32, 62]. We henceforth map to videos

<sup>1</sup>besides lip motion, which is non-injective and therefore insufficient.

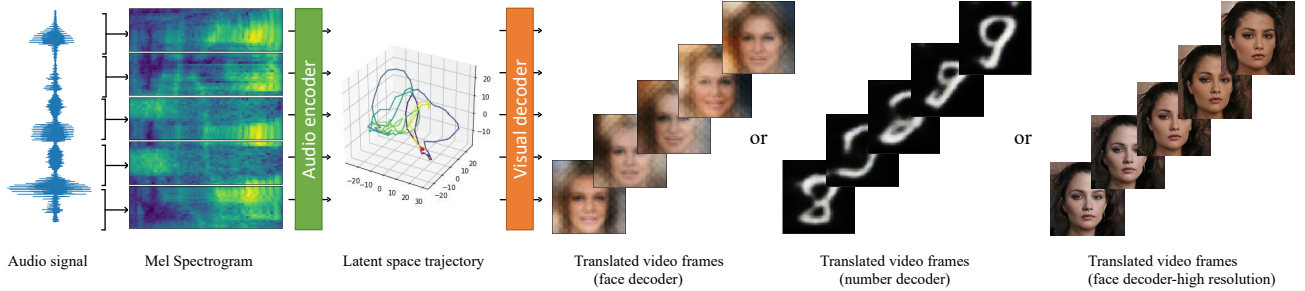


Figure 1. **AudioViewer**: A tool developed towards the long-term goal of helping hearing impaired persons to see what they can not hear. We map an audio stream to video and thereby use faces or numbers for visualizing the high-dimensional audio features intuitively. Different from the principle of lip reading, this can encode general sound and pass on information on the style of spoken language.

that have natural image statistics and a large style variation, such as faces and hand-written digits.

We demonstrate the feasibility of this AudioViewer approach with a working prototype and analyze the success by quantifying a lower bound for the loss of information content as well as showing that words and pronunciation can be distinguished and learned from the generated video features in a user study; much better than from synthesized lip motions because a partial mapping loses important audio features.

**Ethics, risk mitigation, and scope.** Messing with the perceptual system of the study participants by applying sensory substitution bears non-negligible risks that we mitigate by a comparative study design that is approved by our IRB. We show that our computer vision contributions enable a mapping from audio to video that is discriminative and that subjects can learn to better distinguish visualizations. Whether an entire language can be learned will require psychophysical studies controlled by domain experts that can mitigate the risk of side effects on long-term participants.

## 2. Related Work

In the following section, we first review the literature on audio and video generation, with a particular focus on cross-modal models. We then put our approach in context with existing assistive systems.

**Classical audio to video mappings.** Audio to video translation methods have mostly been designed for digital dubbing or lip-syncing facial expressions to spoken audio [6, 13, 29, 38, 45, 53, 55, 68, 75, 76]. Other approaches reconstruct facial attributes, such as gender and ethnicity, from audio and generating matching facial images [67] and map music to facial or body animation [5, 33, 56, 59, 63]. In contrast to our setting, these tasks are typically learned from paired examples, videos with audio lines, e.g., a talking person where the correspondence of lip motion, expressions and facial appearance to the spoken language is used to train the relation between sound and mouth opening. However,

there are multiple sounds that correlate with the same lip and facial motion and others that do not correlate at all. By contrast, our unpaired translation mechanism is designed to map the entire audio spectrum.

**Audio and video generation models.** Image generation models predominantly rely on GAN [19] and VAE [23, 37] formulations. The highest image fidelity is attained with hierarchical models that inject noise and latent codes at various network stages by changing their feature statistics [26, 35]. For audio, only a few methods operate on the raw waveform [31]. It is more common to use spectrograms and to apply convolutional models inspired by the ones used for image generation [2, 12, 24]. We use cross-modal VAE models as a basis to learn the important audio and image features in terms of their frequency.

**Cross-modal latent variable models.** CycleGAN and its variations [60, 77] have considerable success in performing cross-modal unsupervised domain transfer, for medical imaging [22, 65] and audio to visual translation [20], but often encode information as a high-frequency signal that is invisible to the human eye and susceptible to adversarial attacks [8]. An alternative approach involves training a VAE, subject to a cycle-consistency condition [30, 71], but these works were restricted to domain transfers within a single modality. Most similar is the joint audio and video model proposed by Tian et al. [64], which uses a VAE to map between two incompatible latent spaces using supervised alignment of attributes. However, it operates on a word, not phoneme level, and has no mechanism to ensure temporal smoothness nor information throughput. Our contributions address these shortcomings. Relatedly, encoder-decoder and GAN models have been applied to generating video reconstructions of lip movements based on audio data [4, 9, 45, 66, 75, 76], however, due to mapping ambiguities between phonemes and visemes, lip movements are not a reliable source of feedback for learning sound production [3, 16, 42, 47], which we further confirm with our evaluation.

**Deaf speech support tools.** Improvements in speech production for the deaf people have been achieved through non-auditory aids and these improvements persist beyond learning sessions and extend to words not encountered during the sessions [49, 58, 74]. While electrophysiological [21, 36] and haptic learning aids [14] have demonstrated efficacy for improving speech production, such techniques can be more invasive, especially for young children, as compared to visual aids. Elssmann et al. [15] demonstrate visual feedback from the Speech Spectrographic Display (SSD) [58] is equally effective at improving speech production as compared with feedback from a speech-language pathologist. Alternative graphical plots generated from transformed spectral data have been explored by [39, 69, 70], which aim at improving upon spectrograms by creating plots that are more distinguishable with respect to speech parameters. Other methods aim at providing feedback by explicitly estimating vocal tract shapes [50]. In addition, Levis et al. [41] demonstrate that distinguishing between discourse-level intonation (intonation in conversation) and sentence-level intonation (intonation of sentences spoken in isolation) is possible through speech visualization and argues that deaf speech learning could be further improved by incorporating the former. Commercially, products such as the IBM’s Speech Viewer [27] are available to the public. Our image generation approach extends these spectrogram visualization techniques by leveraging the generative ability of VAEs in creating a mapping to a more natural video representation.

**Sensory substitution and audio visualization.** Related to our work is the field of sensory substitution, whereby information from one modality is provided to an individual through a different modality. While many sensory substitution methods focus on substituting visual information into other senses like tactile or auditory stimulation to help visual rehabilitation [18, 25, 44], few methods target substituting auditory modal with visualization. Audio visualization is another field related to our work. Music visualization works generate visualizations of songs such that users can browse songs more efficiently without listening to them [61, 72]. On the learning side, [73] visualize the intonation and volume of each word in speech by the font size enables learning narration strategies. Different from the works mentioned above, our model tries to visualize speech and other audio at the phoneme and sound level with deep learning models instead of selected hand-crafted features.

### 3. Method

Our goal is to translate a one-dimensional audio signal  $\mathbf{A} = (\mathbf{a}_1, \dots, \mathbf{a}_{T_A})$  into a video visualization  $\mathbf{V} = (\mathbf{I}_1, \dots, \mathbf{I}_{T_V})$ , where  $\mathbf{a}_i \in \mathbb{R}$  are sound wave samples recorded over  $T_A$  time steps and  $\mathbf{I}_i$  are images representing the same content over  $T_V$  frames. Supervised training

is not possible in the absence of paired labels.<sup>2</sup> Instead, we start by learning individual audio and video models from datasets without correspondence. These are subsequently linked with an unpaired audio-to-video translation network that conserves high-level properties such as smoothness, regularity, and information loss using cycle-consistency and other unsupervised objectives.

Figure 2 shows the individual steps. The audio encoder  $E_A(\mathbf{a}_i)$  yields a audio latent code  $\mathbf{z}_i \in \mathcal{Z}_A$  and the visual decoder  $D_V(\mathbf{z}_i)$  outputs a corresponding image  $\mathbf{I}_i$ . This produces a video representation of the audio when applied sequentially. Section 3.4 introduces the handling of mismatching latent spaces with a translation network.

**Equalizing sound and video dimensionality.** A first technical problem lies in the higher audio sampling frequency (16000 Hz), that prevents a one-to-one mapping to 25 Hz video. We follow common practice and represent the sound wave with a mel-scaled spectrogram,  $\mathbf{M} = (\mathbf{m}_1, \dots, \mathbf{m}_{T_M})$ ,  $\mathbf{m}_i \in \mathbb{R}^F$ , where  $F = 80$  is the number of filter banks. It is computed via the short-time Fourier transform with a 25 ms Hanning window with 10 ms shifts. In the following, we explain how to map from overlapping segments of length  $T_M = 20$  (covering 200 ms) to corresponding video frames.

#### 3.1. Audio Encoding

Given unlabelled audio and video sequences, we start by learning independent encoder-decoder pairs  $(E_A, D_A)$  for sound and  $(E_V, D_V)$  for video. We use probabilistic VAEs since these do not only learn a compact representation of the latent structure, but also allow us to control the shape of the latent distribution to be a standard normal distribution. Let  $\mathbf{x}$  be a sample from the unlabelled audio set. We optimize over all samples using the VAE objective [37]:

$$\mathcal{L}(\mathbf{x}) = -D_{\text{KL}}(q_\phi(\mathbf{z}|\mathbf{x})||p_\theta(\mathbf{z})) + \mathbb{E}_{q_\phi(\mathbf{z}|\mathbf{x})}(\log p_\theta(\mathbf{x}|\mathbf{z})), \quad (1)$$

with  $D_{\text{KL}}$ , the Kullback-Leibler divergence, and  $q_\phi(\mathbf{z}|\mathbf{x})$  and  $p_\theta(\mathbf{x}|\mathbf{z})$ , the latent code and output domain posterior, respectively. These have a parametric form, with

$$q_\phi(\mathbf{z}|\mathbf{x}) = \mathcal{N}(\boldsymbol{\rho}(\mathbf{x}), \boldsymbol{\omega}^2(\mathbf{x})\mathbf{I}) \quad \text{and} \quad (2)$$

$$p_\theta(\mathbf{x}|\mathbf{z}) = \mathcal{N}(\boldsymbol{\mu}(\mathbf{z}), \boldsymbol{\sigma}^2(\mathbf{z})\mathbf{I}), \quad (3)$$

where  $\boldsymbol{\rho}$  and  $\boldsymbol{\omega}$  are the output of the encoder and  $\boldsymbol{\mu}$  and  $\boldsymbol{\sigma}$  the output of the decoder. We use the SpeechVAE model from Hsu et al. [24] that is widely used for generative sound models.

#### 3.2. Structuring the Audio Encoding

**Content separation.** To better model speech, which we expect to have a higher information content compared to

<sup>2</sup>E.g., speech videos contain paired examples, but only for mapping from speech to lip motion, which we show is insufficient.

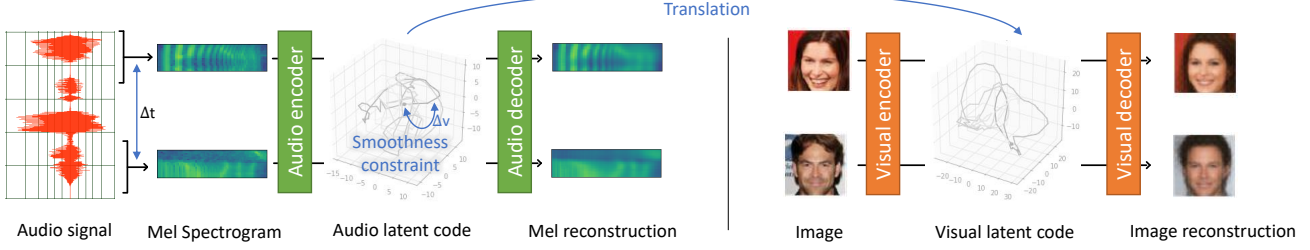


Figure 2. **Overview.** A joint latent encoding is learned with audio and video VAEs that are linked with a translation network and augmented with a smoothness constraint ( $\Delta v$  annotation).

environment sounds, we further disentangle the style, such as gender and dialect, from the content conveyed in phones by leveraging datasets that have phone and speaker annotations. The separation follows that of established audio models [54], the details are provided in the supplemental document. Unless otherwise stated, we map only the audio content for visualization in our experiments.

**Smoothness.** We desire our latent space to change smoothly in time. However, the audio encoder has a small temporal receptive field, encoding time segments of 200ms. This lets encodings of subsequent sounds be encoded to distant latent codes leading to quick visual changes in the decoding. To counteract, we add a temporal smoothness loss on pairs of mel spectrogram segments  $\{\mathbf{M}_{i,1}, \mathbf{M}_{i,2}\}$  sampled at random time steps  $\{t_{i,1}, t_{i,2}\}$  spaced at most 800ms apart. We test two different pair-loss functions to enforce temporal smoothness in the embedded content vectors. First, by making changes in the latent space proportional to changes in time,

$$\mathcal{L}_{p,MSE} = \frac{1}{N} \sum_i (\Delta \hat{\mathbf{z}}_i - \|t_{i,1} - t_{i,2}\|)^2, \quad (4)$$

$\Delta \hat{\mathbf{z}}_i = s_p \cdot \|\mathbf{z}_{i,1} - \mathbf{z}_{i,2}\|$  the distance in the latent space samples obtained from  $\{\mathbf{M}_{i,1}, \mathbf{M}_{i,2}\}$ , scale  $s_p \in \mathbb{R}$  learned to find a scale between time and latent space dimensions. We found it advantageous to measure distances in the logarithmic scale,

$$\mathcal{L}_{p,\log} = \frac{1}{N} \sum_i (\log \Delta \hat{\mathbf{z}}_i - \log \|t_{i,1} - t_{i,2}\|)^2, \quad (5)$$

which lessens the weight for more distant encodings. Our final model uses  $\mathcal{L}_{p,\log}$ . We add this loss to the VAE objective with a weight of  $\lambda_p = 10^3$ .

### 3.3. Image Autoencoder for Video Generation

We experiment with three different video models ranging from low-res to photo-realistic image generation: A linear PCA space, the image DFC-VAE model from Hou et al. [23], and the image Soft-IntroVAE model from Daniel et al. [11]. We use pre-trained models, trained on collections of images. At first, naive unpaired translation is attained by encoding

audio snippets sequentially and concatenating the audio encoder and video decoder of two VAEs with matching latent dimension and the same prior distribution  $p(\mathbf{z})$  over  $\mathbf{z} \in \mathcal{Z}_V$  to generate the frames of the output video.

### 3.4. Linking Audio and Visual Spaces

One of our key contributions is to meaningfully link the audio and video domain without having paired examples. The naive concatenation explained in the previous section leads to low-quality results because smoothness in the latent space does not necessarily lead to smoothness in the output video, latent dimensions often do not match, and both encoders are only approximations to the true distribution.

When latent spaces have the same dimension, i.e., with [23] as visual model, we utilize a shared latent space and refine the weights of the video model to bridge structural differences. For [11], which has a larger latent space and is costly to train, we use a pre-trained model. To nevertheless link audio and video latent spaces, we introduce a translation network  $T(\mathbf{z})$  that maps the latent code  $\mathbf{z}$  of the input audio segment to the visual latent variable  $T(\mathbf{z})$ . Figure 3, visualizes this mapping and how the visual decoder  $D_V$  subsequently decodes  $T(\mathbf{z})$  to the output image  $I$ .

Since our setting is unpaired we have to resort to self-supervised losses for modeling high-level constraints on auxiliary tasks instead of supervised learning. We explain them in the order of basic to more complex. First, to be a proper mapping, the range of  $T(\mathbf{z})$  should be in the domain of the video decoder. Since the visual latent space fulfills the standard Gaussian distribution, we minimize its negative log-likelihood,

$$\mathcal{L}_{reg} = \lambda_{reg} \|T(\mathbf{z})\|^2, \quad (6)$$

where  $\lambda_{reg} = 1.0$ . Second, we minimize a lower bound on the information loss with the cycle consistency loss,

$$\mathcal{L}_{cycle} = \lambda_{cycle} \|E_V(D_V(T(\mathbf{z}))) - T(\mathbf{z})\|, \quad (7)$$

that measures the difference between  $T(\mathbf{z})$  and the reconstructed encoding of the generated image  $I$  via visual encoder  $E_V$  and is weighted by  $\lambda_{cycle} = 1.0$ .



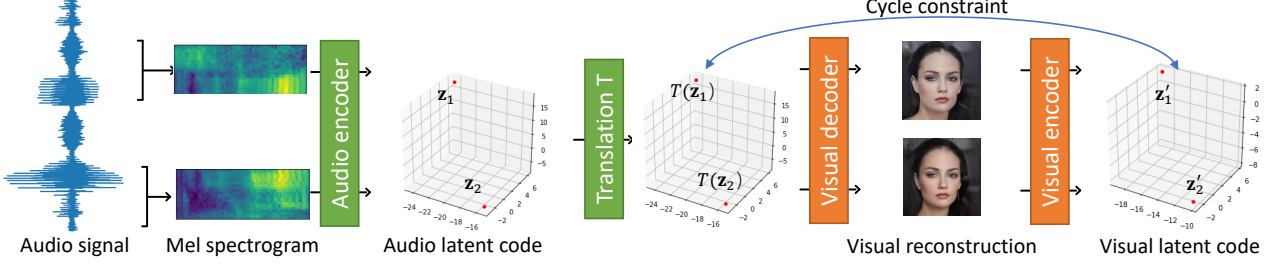


Figure 3. **Cycle constraint.** We apply a cycle constraint to ensure that the signal is preserved through video decoding and encoding.

At the same time, consistent with Section 3.2, the changes in the generated image should be smooth. We ensure this with an additional temporal smoothness loss

$$\mathcal{L}_{\text{smooth}} = \lambda_{\text{smooth}} \frac{1}{N} \sum_i (\log(\|I_{i,1} - I_{i,2}\|_{\text{smooth}}) - \log\|t_{i,1} - t_{i,2}\|)^2. \quad (8)$$

To further facilitate training of our multi-stage architecture, we also enforce a distance preserving loss

$$\mathcal{L}_{\text{iso}} = \lambda_{\text{iso}} \frac{1}{N} \sum_i (\log\|T(\mathbf{z}_{i,1}) - T(\mathbf{z}_{i,2})\| - \log(\|(\mathbf{z}_{i,1} - \mathbf{z}_{i,2})\| s_{\text{iso}}))^2. \quad (9)$$

As in Section 3.2, we input the mel spectrogram segment pairs with random time steps  $\{t_{i,1}, t_{i,2}\}$ , where  $i$  represents the  $i$ th input pair. And  $\lambda_{\text{iso}} = 1.0$ ,  $s_{\text{iso}} = 5.0$ ,  $\lambda_{\text{smooth}} = 5.0$  and  $s_{\text{smooth}} = 0.001$ .

Note that neither of these self-supervised losses requires annotation. It therefore applies to environment sounds and could easily be finetuned for any language or dialect as long as an audio recording is available.

To measure the throughput of the entire system when using  $T$  together with [11], we train a back-translation network  $T^\dagger$  to reconstruct the input audio with the loss

$$\mathcal{L}_{\text{back}} = \|D_A(T^\dagger(E_V(D_V(T(E_A(\mathbf{a}_i)))))) - \mathbf{a}_i\|^2. \quad (10)$$

This inverse mapping training is a postprocess, only needed for evaluating throughput.

## 4. Experiments

In the following, we show qualitatively and quantitatively that AudioViewer conveys important audio features via visualizations of portraits or numbers, that it applies to speech and environment sounds, that the task cannot be solved with simpler baselines, and that it outperforms a mapping to lip motion [76]. We provide additional results and implementation details in the supplemental videos and document.

**Quantitative metrics.** We compare latent embeddings by the Euclidean distance, mel spectrogram with the signal to noise ratio (SNR), and smoothness is measured as the change in latent space position.

**Perceptual study.** We perform a user study to analyze the human capability to perceive the translated audio content. Some results may be subjective and we therefore report statistics over 29 questions answered by 10-22 participants for each of the examined approaches. The study details are given in the supplemental document.

**Baselines.** We compare to the most straight-forward speech to video translation, by mapping to lip and facial motion using the recent MakeItTalk method [76]. To show that simpler approaches are insufficient, we experiment with simpler variants of our approach and principal component analysis (PCA) as a further baseline. PCA yields a projection matrix  $\mathbf{W}$  that rotates the training samples  $\mathbf{u}_i$  by  $\mathbf{z}_i = \mathbf{W}\mathbf{u}_i$  to have diagonal covariance matrix  $\Sigma$  and maximal variance. We use the reduced PCA version, where  $\mathbf{W}$  maps to a  $d$ -dimensional space.

In addition, we ablate the impact of our latent space priors and training strategies introduced in sections 3.2 and 3.4 as well as when disabling the style-content disentangling.

A further important factor is the impact of the video domain, for which we compare digits vs. faces at the same resolution and low vs. high-resolution faces.

**Audio Datasets.** We use the TIMIT dataset [17] for learning speech embeddings. It contains 5.4 hours of audio recordings (16 bit, 16 kHz) as well as time-aligned orthographic, phonetic and word transcriptions for 630 speakers of eight major dialects of American English, each reading ten phonetically rich sentences. We use the training split (462/50/24 non-overlapping speakers) of the KALDI toolkit [52]. The phonetic annotation is only used at audio encoder training time and as ground truth for the user study.

In addition, we report how well a model trained on speech generalizes to environmental sounds on ESC-50 dataset [51].

**Image Datasets.** To test what kind of visualization is best for humans to perceive the translated audio, we train and test our model on three image datasets: The face attributes dataset CelebA-HQ [34] (29000/1000 images for



Figure 4. **Word analysis.** Instances (different rows) of the same words are encoded with a similar video sequence (single row) even though spoken by different speakers.

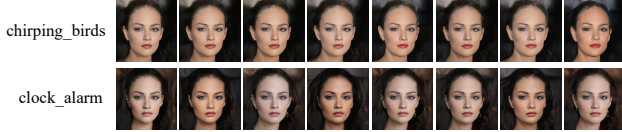


Figure 5. **Environment sounds visualization.** Although not trained for it, our approach also visualizes natural sounds. Here showing a clear difference between a chirping bird and an alarm clock.

train/val respectively) and CelebA [43] (162770/19962 images for train/val respectively), the MNIST [40] datasets (60000/10000 images for train/val respectively). All shown results are with the high-res [11] decoder unless otherwise mentioned.

**Runtime** The supplemental video contains a live demo. The AudioViewer using [23] is real-time capable, the inference time for a frame is 5 ms on an i7-9700KF CPU at 3.60GHz with a single NVIDIA GeForce RTX 2080 Ti.

#### 4.1. Visual Quality and Phonetics

A meaningful audio translation should encode similar sounds with similar visuals. Figure 6 depicts such similarity and dissimilarity on the first 200 ms of a spoken word since these can be visualized with a single video frame. This figure compares the content encoding to MNIST and faces; both are well suited to distinguish sounds. The same word (column) has high visual similarity across different speakers (F#: female, M#: male; # the speaker ID) and dialects (D#: while words starting with different sounds are visually different. Multiple frames of entire words are shown in Fig. 4. Our user study and supplemental document analyze their differences in more detail and on entire sentences.

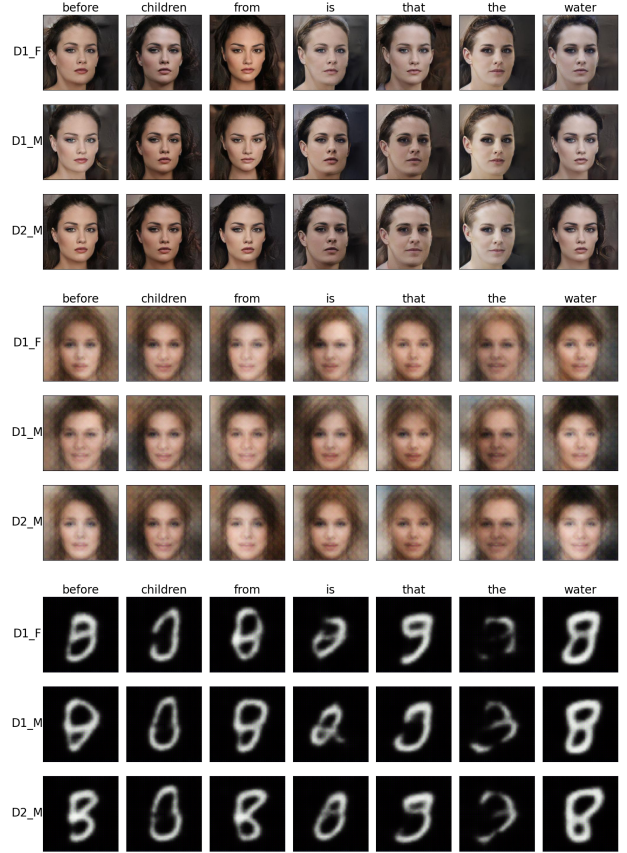


Figure 6. **Phoneme similarity.** The first phone of different words are distinctive (columns) while the speakers has a small influence (rows). This is consistent across image domains (Top to bottom: CelebA high-res, CelebA low-res, and MNIST).



Figure 7. **Throughput.** A lower bound on the information throughput as the loss of mapping from audio to video and back. Playing the smoothed audio shows that it is still recognizable.

Although trained entirely on speech, our low-level formulation at the level of sounds enables AudioViewer to also visualize environment sounds. Figure 5 gives two examples.

#### 4.2. Information Throughput

It is difficult to quantify the information throughput from audio to video as no ground truth is available. We use the learned encoder and decoder to map from audio to video and back as a lower bound. This cyclic pattern lets us quantify the loss of information as the distance of the starting point

Table 1. **Throughput lower bound.** The throughput estimate from audio to video with AudioViewer shows that the cycle consistency improves greatly while the enforcement of additional constraints with  $\mathcal{L}_{p,\log}$ , and  $\mathcal{L}_{rr}$ , takes only a small dip.

Audio models	Visual models	SNR(dB)
Audio PCA	Visual PCA	23.37
SpeechVAE [24]	DFC-VAE on CelebA	1.65
	DFC-VAE on MNIST	2.01
	DFC-VAE on CelebA (refined w/ $\mathcal{L}_{cycle}$ )	<b>4.43</b>
	DFC-VAE on MNIST (refined w/ $\mathcal{L}_{cycle}$ )	0.78
SpeechVAE w/ $\mathcal{L}_{p,\log}$ , $\mathcal{L}_{rr}$ , dim=256	DFC-VAE on CelebA	0.84
	DFC-VAE on MNIST	0.81
	DFC-VAE on CelebA (refined w/ $\mathcal{L}_{cycle}$ )	<b>4.16</b>
	DFC-VAE on MNIST (refined w/ $\mathcal{L}_{cycle}$ )	3.68
	Soft-Intro VAE on CelebA_HR (refined w/ $\mathcal{L}_{cycle}$ )	2.01

Table 2. **Audio throughput vs. smoothness.** The SNR of the autoencoder drops with the additional constraints we enforce (smoothness and disentanglement). This is a trade-off for improving velocity, acceleration, and interpretability.

Audio models	SNR (dB)	Velocity ( $s^{-1}$ )	Acc. ( $s^{-2}$ )
Audio PCA	<b>23.37</b>	329.02	13395.11
SpeechVAE [24]	21.89	<b>280.09</b>	<b>11648.17</b>
SpeechVAE w/ $\mathcal{L}_{p,\log}$	<b>19.89</b>	108.89	3052.19
SpeechVAE w/ $\mathcal{L}_{rr}$	7.73	80.80	2947.70
SpeechVAE w/ $\mathcal{L}_{rr}, \mathcal{L}_{p,\log}$	6.20	<b>59.78</b>	<b>1530.81</b>
SpeechVAE w/ $\mathcal{L}_{rr}, \mathcal{L}_{p,\log}$ , dim=256	6.28	65.63	1757.95

to the reconstructed audio. Figure 7 gives an example and Table 1 summarizes relations quantitatively. The difference can also be analyzed qualitatively by listening and comparing the original and reconstructed audio samples, which are still recognizable for our full model. We found this throughput an important measure that correlated with performance in user studies and enabled us to tune hyperparameters without performing an expensive user study for each configuration.

Note that the information throughput rivals other constraints such as smoothness. The goal is therefore to strike the best compromise. For instance, PCA attains the highest reconstruction accuracy but has poor smoothness properties (Table 2) and does not strike along the other dimensions. The disentangled space (lower half of Table 1) has a relatively low effect on the SNR, a reduction from 4.43 to 4.16, while providing improved interpretability. MNIST proved less stable to train and does not fair well with the cycle loss, perhaps due to a lower dimensionality that mismatches with the higher-dimensional audio encoding. The high-res CelebA model yields a lower SNR, likely because information is lost in the deeper network and the smoothness loss affects high-frequency details differently.

### 4.3. Temporal Smoothness Effectiveness

Mapping from audio to video with VAEs without constraints and PCA leads to choppy results. Table 2 shows that this corresponds to mean latent space velocities above  $300 s^{-1}$ . It shows that the tested simpler solutions are in-

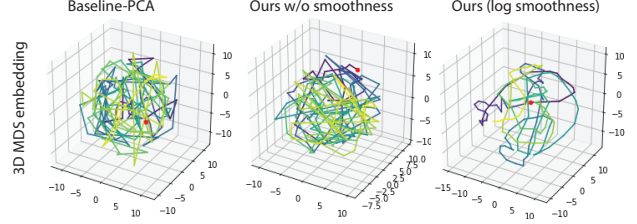


Figure 8. **Smoothness evaluation** by plotting the latent embedding of an audio snippet in 3D via dimensionality reduction. **Left:** Without smoothness constraint, consecutive audio sample embeddings are scattered. **Right:** Our full model leads to smoother trajectories.

sufficient. We visualize the gain in smoothness in Figure 8 by plotting the high-dimensional latent trajectory embedded into three dimensions using multi-dimensional scaling (MDS) [10]. The gain is similar for all of the proposed variants. The supplemental videos show how the smoothness eases information perception.

### 4.4. Visual Domain Influence

Earlier work [7, 28] suggests that faces are suitable for representing high-dimensional data. Our experiments support this finding for the task at hand, in that the measurable information content is larger. The SNR of the jointly trained CelebA models is larger than the MNIST models. Figure 6 indicates that facial models are richer in information. The user study explained in the following shows that using the higher-resolution image generator leads to slight improvements even though the throughput is lower. The throughput estimate is hence good for tuning hyperparameters of the same model but is influenced by the video encoder and audio decoder which can lead to mismatching scores when changing these.

### 4.5. User Study I - Discriminating Sounds

We analyze the gain from a disentangled latent space vs. a combined one and the difference of using faces or digits for visualization with a user study among 45 participants answering 29 questions, with the same question repeated for four visualization techniques, including the state-of-the-art lip synchronisation method [76].

**Identifying and distinguishing sounds.** Our user study analyzes the ability to distinguish between visualizations of different sounds, similar to the ones show in Figure 6 and the results are shown in Table 3. Overall, the users were able to correctly recognize visualizations for the same sound with an accuracy of 86.4% for the high-res CelebA content model and 85.0% vs. 79.7% for the low-res CelebA and MNIST content models, respectively. Broken down by tasks, users for the CelebA model achieve a better accuracy of 87.9%



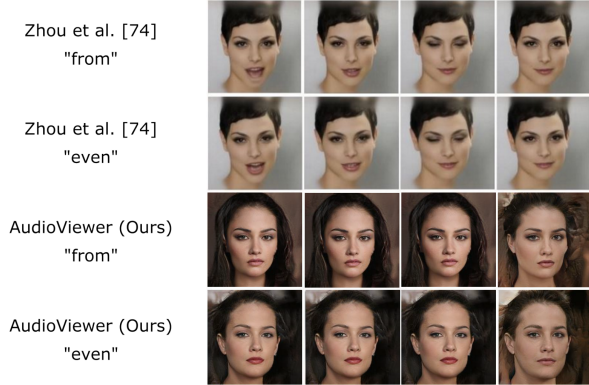


Figure 9. **Comparison to lip-sync by [76].** While the lip synchronization looks very similar, the two words are clearly distinguishable in the AudioViewer visualizations.

Table 3. **User Study I results.** User answer accuracy in percent ( $\pm$  std.) for distinguishing between visualizations of different sounds, broken down by question type and phone-pairs vs. words.

Dataset	CelebA	CelebA	MNIST	Zhou et al. [76]
Resolution	(high-res)	(low-res)	(low-res)	(high-res)
Matching questions	<b>87.9 <math>\pm</math> 10.5</b>	84.5 $\pm$ 13.8	77.4 $\pm$ 10.6	65.6 $\pm$ 13.3
Grouping questions	<b>85.7 <math>\pm</math> 8.3</b>	85.2 $\pm$ 8.8	80.8 $\pm$ 8.4	39.5 $\pm$ 14.5
Phone-pairs	87.0 $\pm$ 11.6	85.7 $\pm$ 11.2	<b>91.8 <math>\pm</math> 9.2</b>	69.5 $\pm$ 19.4
Words	<b>86.0 <math>\pm</math> 6.9</b>	84.5 $\pm$ 8.6	73.8 $\pm$ 7.2	39.4 $\pm$ 10.7
<b>Overall</b>	<b>86.4 <math>\pm</math> 6.8</b>	85.0 $\pm$ 6.8	79.7 $\pm$ 6.5	47.7 $\pm$ 10.0

in correctly matching one of two visualizations against a reference (random guessing yields 50%), while for the task of grouping four visualizations into pairs, users achieved an accuracy of 85.7 % (random guessing yields 33.3%).

In comparison to the lip synchronisation of Zhou et al. [76] AudioViewer enables a user to distinguish sounds significantly better. This is due to the almost identical lip motion for different phonemes (e.g. "d", "t" and "n") which makes them indistinguishable. Figure 9 shows such a case of two words that look similar in lip motion but are clearly distinguishable in the AudioViewer visualizations.

**Latent space disentanglement.** Visualizing the style and content part separately with our full model significantly improves recognition scores. The disentangled face model increases the accuracy for distinguishing between speakers of a different sex from  $43.3 \pm 8.9\%$  to  $78.0 \pm 10.8\%$  and speakers of different dialects from  $39.6 \pm 24.9\%$  to  $56.7 \pm 22.1\%$ . An AudioViewer prototype should therefore use the full model and show separate visual decodings side by side or have the option to switch between content and style visualization. The user study is reported in full in the supplemental document.

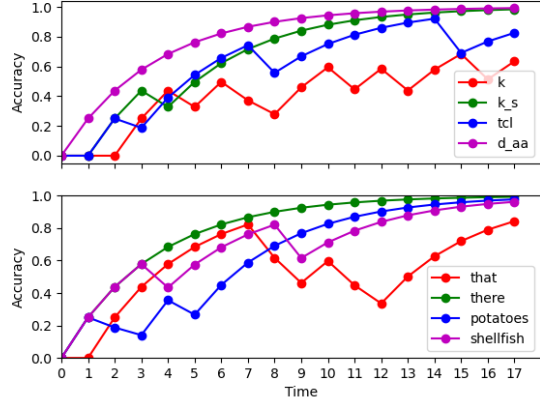


Figure 10. **User Study II results.** Subjects learn over time to distinguish phones (top) and words (bottom). As expected, less distinct sounds such as  $k_s$  and  $k$  are harder to learn. Accuracy is plotted as the moving average of the success rate over trials.

#### 4.6. User Study II - Learning Sounds

In this second study, four phones/words spoken by different speakers with different dialects and the same gender were shown sequentially to the subject. The study task was to select the visualized sound/word from the four choices, e.g. phones  $k$ ,  $k_s$ ,  $tcl$ ,  $d_{aa}$ . After each selection, the correct answer is disclosed as a feedback mechanism. Figure 10 shows the learning curves for one subject with respect to each sound/word. Their increasing trajectory reflects how the subject learns to recognize the same sound spoken by different people over time. The entire study and study details are included in the supplemental document.

#### 5. Limitations and Future Work

When presented with our visualizations the first time, users are unsure of what features they should focus on to distinguish. Our Study II shows that this improves with learning but similar sounds, such as  $k$  and  $k_s$  remain ambiguous. There is room for improving the expressiveness and for making the visual language more intuitive. Moreover, the visualization of environment sounds lose higher frequency components since the audio models are trained on a speech dataset. To create a more natural mapping, we plan to map to lip motion for spoken sounds that are captured in the lip motion while maintaining the proposed general encoding for those that are not and for environment sounds.

#### 6. Conclusion

We presented AudioViewer, a learning-based approach for visualizing audio, including speech and sounds, via generative models trained in the absence of paired examples. It can visualize sounds on faces and digits and outperforms all



baselines, including state-of-the-art lip synchronization in distinctiveness. Our face visualizations retain more information than lip motion or digits alone. Our proof of concept AudioViewer demo shows the feasibility of visualizing speech in real-time. We hope that our sensory substitution approach will catalyze the development of future tools for assisting people with auditorial handicaps.

## References

- [1] Geoffrey K Aguirre, E Zarahn, and M D’esposito. An area within human ventral cortex sensitive to “building” stimuli: evidence and implications. *Neuron*, 21(2):373–383, 1998. 1
- [2] Jean-Pierre Briot, Gaëtan Hadjeres, and François-David Pachet. Deep learning techniques for music generation—a survey. *arXiv preprint arXiv:1709.01620*, 2017. 2
- [3] Luca Cappelletta and Naomi Harte. Phoneme-to-viseme mapping for visual speech recognition. In *ICPRAM* (2), pages 322–329, 2012. 2
- [4] Lele Chen, Zhiheng Li, Ross K Maddox, Zhiyao Duan, and Chenliang Xu. Lip movements generation at a glance. In *Proceedings of the European Conference on Computer Vision (ECCV)*, pages 520–535, 2018. 2
- [5] Lele Chen, Sudhanshu Srivastava, Zhiyao Duan, and Chenliang Xu. Deep cross-modal audio-visual generation. In *Proceedings of the on Thematic Workshops of ACM Multimedia 2017*, Thematic Workshops ’17, page 349–357, New York, NY, USA, 2017. Association for Computing Machinery. 2
- [6] Lele Chen, Haitian Zheng, Ross Maddox, Zhiyao Duan, and Chenliang Xu. Sound to visual: Hierarchical cross-modal talking face generation. In *Proceedings of the IEEE/CVF Conference on Computer Vision and Pattern Recognition (CVPR) Workshops*, June 2019. 1, 2
- [7] Herman Chernoff. The use of faces to represent points in k-dimensional space graphically. *Journal of the American statistical Association*, 68(342):361–368, 1973. 1, 7
- [8] Casey Chu, Andrey Zhmoginov, and Mark Sandler. CycleGAN, a master of steganography. *arXiv preprint arXiv:1712.02950*, 2017. 2
- [9] Joon Son Chung, Amir Jamaludin, and Andrew Zisserman. You said that? *arXiv preprint arXiv:1705.02966*, 2017. 2
- [10] Michael AA Cox and Trevor F Cox. Multidimensional scaling. In *Handbook of data visualization*, pages 315–347. Springer, 2008. 7
- [11] Tal Daniel and Aviv Tamar. Soft-introvae: Analyzing and improving the introspective variational autoencoder. In *Proceedings of the IEEE/CVF Conference on Computer Vision and Pattern Recognition*, pages 4391–4400, 2021. 4, 5, 6
- [12] Hao-Wen Dong, Wen-Yi Hsiao, Li-Chia Yang, and Yi-Hsuan Yang. Musegan: Multi-track sequential generative adversarial networks for symbolic music generation and accompaniment. In *Thirty-Second AAAI Conference on Artificial Intelligence*, 2018. 2
- [13] Amanda Duarte, Francisco Roldan, Miquel Tubau, Janna Escur, Santiago Pascual, Amaia Salvador, Eva Moledano, Kevin McGuinness, Jordi Torres, and Xavier Giro-i Nieto. Wav2pix: speech-conditioned face generation using generative adversarial networks. In *IEEE International Conference on Acoustics, Speech and Signal Processing (ICASSP)*, volume 3, 2019. 1, 2
- [14] Silvio P Eberhardt, Lynne E Bernstein, David C Coulter, and Laura A Hunckler. Omar a haptic display for speech perception by deaf and deaf-blind individuals. In *Proceedings of IEEE Virtual Reality Annual International Symposium*, pages 195–201. IEEE, 1993. 3
- [15] Sharon F Elssmann and Jean E Maki. Speech spectrographic display: use of visual feedback by hearing-impaired adults during independent articulation practice. *American Annals of the Deaf*, pages 276–279, 1987. 3
- [16] Adriana Fernandez-Lopez and Federico M Sukno. Optimizing phoneme-to-viseme mapping for continuous lip-reading in spanish. In *International Joint Conference on Computer Vision, Imaging and Computer Graphics*, pages 305–328. Springer, 2017. 2
- [17] John S Garofolo. Timit acoustic phonetic continuous speech corpus. *Linguistic Data Consortium*, 1993, 1993. 5
- [18] Louis H Goldish and Harry E Taylor. The optacon: A valuable device for blind persons. *Journal of Visual Impairment & Blindness*, 68(2):49–56, 1974. 3
- [19] Ian Goodfellow, Jean Pouget-Abadie, Mehdi Mirza, Bing Xu, David Warde-Farley, Sherjil Ozair, Aaron Courville, and Yoshua Bengio. Generative adversarial nets. In *Advances in neural information processing systems*, pages 2672–2680, 2014. 2
- [20] Wangli Hao, Zhaoxiang Zhang, and He Guan. Cmcgan: A uniform framework for cross-modal visual-audio mutual generation. In *Thirty-Second AAAI Conference on Artificial Intelligence*, 2018. 2
- [21] William J Hardcastle, Fiona E Gibbon, and Wilf Jones. Visual display of tongue-palate contact: electropalatography in the assessment and remediation of speech disorders. *International Journal of Language & Communication Disorders*, 26(1):41–74, 1991. 3
- [22] Yuta Hiasa, Yoshito Otake, Masaki Takao, Takumi Matsuoka, Kazuma Takashima, Aaron Carass, Jerry L Prince, Nobuhiko Sugano, and Yoshinobu Sato. Cross-modality image synthesis from unpaired data using cycleGAN. In *International workshop on simulation and synthesis in medical imaging*, pages 31–41. Springer, 2018. 2
- [23] X. Hou, L. Shen, K. Sun, and G. Qiu. Deep feature consistent variational autoencoder. In *2017 IEEE Winter Conference on Applications of Computer Vision (WACV)*, pages 1133–1141, 2017. 2, 4, 6
- [24] Wei-Ning Hsu, Yu Zhang, and James Glass. Learning latent representations for speech generation and transformation. In *Interspeech*, pages 1273–1277, 2017. 2, 3, 7
- [25] Di Hu, Dong Wang, Xuelong Li, Feiping Nie, and Qi Wang. Listen to the image. In *Proceedings of the IEEE/CVF Conference on Computer Vision and Pattern Recognition (CVPR)*, June 2019. 3
- [26] Xun Huang and Serge Belongie. Arbitrary style transfer in real-time with adaptive instance normalization. In *Proceedings of the IEEE International Conference on Computer Vision*, pages 1501–1510, 2017. 2

- [27] IBM. Speech viewer iii, 2004. 3
- [28] Robert JK Jacob and Howard E Egeth. The face as a data display. *Human Factors*, 18(2):189–200, 1976. 1, 7
- [29] Amir Jamaludin, Joon Son Chung, and Andrew Zisserman. You said that?: Synthesising talking faces from audio. *International Journal of Computer Vision*, 127(11):1767–1779, 2019. 2
- [30] Ananya Harsh Jha, Saket Anand, Maneesh Singh, and VSR Veeravasarapu. Disentangling factors of variation with cycle-consistent variational auto-encoders. In *European Conference on Computer Vision*, pages 829–845. Springer, 2018. 2
- [31] Herman Kamper. Truly unsupervised acoustic word embeddings using weak top-down constraints in encoder-decoder models. In *ICASSP 2019-2019 IEEE International Conference on Acoustics, Speech and Signal Processing (ICASSP)*, pages 6535–6539. IEEE, 2019. 2
- [32] Nancy Kanwisher, Damian Stanley, and Alison Harris. The fusiform face area is selective for faces not animals. *Neuroreport*, 10(1):183–187, 1999. 1
- [33] Tero Karras, Timo Aila, Samuli Laine, Antti Herva, and Jaakko Lehtinen. Audio-driven facial animation by joint end-to-end learning of pose and emotion. *ACM Transactions on Graphics (TOG)*, 36(4):1–12, 2017. 2
- [34] Tero Karras, Timo Aila, Samuli Laine, and Jaakko Lehtinen. Progressive growing of gans for improved quality, stability, and variation. *arXiv preprint arXiv:1710.10196*, 2017. 5
- [35] Tero Karras, Samuli Laine, and Timo Aila. A style-based generator architecture for generative adversarial networks. In *Proceedings of the IEEE Conference on Computer Vision and Pattern Recognition*, pages 4401–4410, 2019. 2
- [36] William F Katz and Sonya Mehta. Visual feedback of tongue movement for novel speech sound learning. *Frontiers in human neuroscience*, 9:612, 2015. 3
- [37] Diederik P Kingma and Max Welling. Auto-encoding variational bayes. *arXiv preprint arXiv:1312.6114*, 2013. 2, 3
- [38] Prajwal KR, Rudrabha Mukhopadhyay, Jerin Philip, Abhishek Jha, Vinay Nambodiri, and CV Jawahar. Towards automatic face-to-face translation. In *Proceedings of the 27th ACM International Conference on Multimedia*, pages 1428–1436, 2019. 2
- [39] Bernd J Kröger, Peter Birkholz, Rüdiger Hoffmann, and Helen Meng. Audiovisual tools for phonetic and articulatory visualization in computer-aided pronunciation training. In *Development of multimodal interfaces: Active listening and synchrony*, pages 337–345. Springer, 2010. 3
- [40] Yann LeCun, Léon Bottou, Yoshua Bengio, and Patrick Haffner. Gradient-based learning applied to document recognition. *Proceedings of the IEEE*, 86(11):2278–2324, 1998. 6
- [41] John Levis and Lucy Pickering. Teaching intonation in discourse using speech visualization technology. *System*, 32(4):505–524, 2004. 3
- [42] Björn Lidenstam and Jonas Beskow. Visual phonemic ambiguity and speechreading. *Journal of Speech, Language, and Hearing Research*, 2006. 2
- [43] Ziwei Liu, Ping Luo, Xiaogang Wang, and Xiaoou Tang. Deep learning face attributes in the wild. In *Proceedings of International Conference on Computer Vision (ICCV)*, December 2015. 6
- [44] Shachar Maidenbaum, Sami Abboud, and Amir Amedi. Sensory substitution: Closing the gap between basic research and widespread practical visual rehabilitation. *Neuroscience & Biobehavioral Reviews*, 41:3–15, 2014. 3
- [45] Rayhane Mama, Marc S. Tyndel, Hashiam Kadhim, Cole Clifford, and Ragavan Thurairatnam. Nwt: Towards natural audio-to-video generation with representation learning, 2021. 1, 2
- [46] Elon Musk et al. An integrated brain-machine interface platform with thousands of channels. *Journal of medical Internet research*, 21(10):e16194, 2019. 1
- [47] Jacob L Newman, Barry-John Theobald, and Stephen J Cox. Limitations of visual speech recognition. In *Auditory-Visual Speech Processing 2010*, 2010. 2
- [48] Kuniaki Noda, Yuki Yamaguchi, Kazuhiro Nakadai, Hiroshi G Okuno, and Tetsuya Ogata. Audio-visual speech recognition using deep learning. *Applied Intelligence*, 42(4):722–737, 2015. 1
- [49] AM Öster. Teaching speech skills to deaf children by computer-based speech training. *STL-Quarterly Progress and Status Report*, 36(4):67–75, 1995. 1, 3
- [50] Sang H Park, Dong J Kim, Jae H Lee, and Tae S Yoon. Integrated speech training system for hearing impaired. *IEEE Transactions on Rehabilitation Engineering*, 2(4):189–196, 1994. 3
- [51] Karol J Piczak. Esc: Dataset for environmental sound classification. In *Proceedings of the 23rd ACM international conference on Multimedia*, pages 1015–1018, 2015. 5
- [52] Daniel Povey, Arnab Ghoshal, Gilles Boulianne, Lukas Burget, Ondrej Glembek, Nagendra Goel, Mirko Hannemann, Petr Motlicek, Yanmin Qian, Petr Schwarz, et al. The kald speech recognition toolkit. In *IEEE 2011 workshop on automatic speech recognition and understanding*, number CONF. IEEE Signal Processing Society, 2011. 5
- [53] K R Prajwal, Rudrabha Mukhopadhyay, Vinay P. Nambodiri, and C.V. Jawahar. A lip sync expert is all you need for speech to lip generation in the wild. In *Proceedings of the 28th ACM International Conference on Multimedia*, MM ’20, page 484–492, New York, NY, USA, 2020. Association for Computing Machinery. 2
- [54] Kaizhi Qian, Yang Zhang, Shiyu Chang, Xuesong Yang, and Mark Hasegawa-Johnson. Autovc: Zero-shot voice style transfer with only autoencoder loss. In *International Conference on Machine Learning*, pages 5210–5219. PMLR, 2019. 4
- [55] Najmeh Sadoughi and Carlos Busso. Speech-driven expressive talking lips with conditional sequential generative adversarial networks. *IEEE Transactions on Affective Computing*, 2019. 1, 2
- [56] Eli Shlizerman, Lucio Dery, Hayden Schoen, and Ira Kemelmacher-Shlizerman. Audio to body dynamics. In *Proceedings of the IEEE Conference on Computer Vision and Pattern Recognition*, pages 7574–7583, 2018. 2

- [57] George Sperling. The information available in brief visual presentations. *Psychological monographs: General and applied*, 74(11):1, 1960. [1](#)
- [58] Larkin W Stewart L and Houde R. A real-time sound spectrograph with implications for speech training for the deaf. In *IEEE International Conference Accoustics Speech and Signal Processing*, 1976. [1](#), [3](#)
- [59] Supasorn Suwajanakorn, Steven M Seitz, and Ira Kemelmacher-Shlizerman. Synthesizing obama: learning lip sync from audio. *ACM Transactions on Graphics (TOG)*, 36(4):1–13, 2017. [2](#)
- [60] Yaniv Taigman, Adam Polyak, and Lior Wolf. Unsupervised cross-domain image generation. *arXiv preprint arXiv:1611.02200*, 2016. [2](#)
- [61] Takumi Takahashi, Satoru Fukayama, and Masataka Goto. Instrudiver: A music visualization system based on automatically recognized instrumentation. In *ISMIR*, pages 561–568, 2018. [3](#)
- [62] Michael J Tarr and Isabel Gauthier. Ffa: a flexible fusiform area for subordinate-level visual processing automatized by expertise. *Nature neuroscience*, 3(8):764–769, 2000. [1](#)
- [63] Sarah Taylor, Taehwan Kim, Yisong Yue, Moshe Mahler, James Krahe, Anastasio Garcia Rodriguez, Jessica Hodgins, and Iain Matthews. A deep learning approach for generalized speech animation. *ACM Transactions on Graphics (TOG)*, 36(4):1–11, 2017. [2](#)
- [64] Yingtao Tian and Jesse Engel. Latent translation: Crossing modalities by bridging generative models. *arXiv preprint arXiv:1902.08261*, 2019. [2](#)
- [65] Oleksandra Tmenova, Rémi Martin, and Luc Duong. Cyclegan for style transfer in x-ray angiography. *International journal of computer assisted radiology and surgery*, 14(10):1785–1794, 2019. [2](#)
- [66] Konstantinos Vougioukas, Stavros Petridis, and Maja Pantic. End-to-end speech-driven facial animation with temporal gans. *arXiv preprint arXiv:1805.09313*, 2018. [2](#)
- [67] Yandong Wen, Rita Singh, and Bhiksha Raj. Reconstructing faces from voices. *arXiv preprint arXiv:1905.10604*, 2019. [2](#)
- [68] Olivia Wiles, A Sophia Koepke, and Andrew Zisserman. X2face: A network for controlling face generation using images, audio, and pose codes. In *Proceedings of the European Conference on Computer Vision (ECCV)*, pages 670–686, 2018. [1](#), [2](#)
- [69] Wang Xu, Xue Lifang, Yang Dan, and Han Zhiyan. Speech visualization based on robust self-organizing map (rsom) for the hearing impaired. In *2008 International Conference on BioMedical Engineering and Informatics*, volume 2, pages 506–509. IEEE, 2008. [3](#)
- [70] Dan Yang, Bin Xu, and Xu Wang. Speech visualization based on improved spectrum for deaf children. In *2010 Chinese Control and Decision Conference*, pages 4377–4380. IEEE, 2010. [3](#)
- [71] Dongsuk Yook, Seong-Gyun Leem, Keonnyeong Lee, and In-Chul Yoo. Many-to-many voice conversion using cycle-consistent variational autoencoder with multiple decoders. In *Proc. Odyssey 2020 The Speaker and Language Recognition Workshop*, pages 215–221, 2020. [2](#)
- [72] Kazuyoshi Yoshii and Masataka Goto. Music thumbnailer: Visualizing musical pieces in thumbnail images based on acoustic features. In *ISMIR*, pages 211–216, 2008. [3](#)
- [73] Linping Yuan, Yuanzhe Chen, Siwei Fu, Aoyu Wu, and Huamin Qu. Speechlens: A visual analytics approach for exploring speech strategies with textural and acoustic features. In *2019 IEEE International Conference on Big Data and Smart Computing (BigComp)*, pages 1–8. IEEE, 2019. [3](#)
- [74] Cindy M Zaccagnini and Shirin D Antia. Effects of multisensory speech training and visual phonics on speech production of a hearing-impaired child. *Journal of Childhood Communication Disorders*, 15(2):3–8, 1993. [1](#), [3](#)
- [75] Hang Zhou, Yu Liu, Ziwei Liu, Ping Luo, and Xiaogang Wang. Talking face generation by adversarially disentangled audio-visual representation. In *Proceedings of the AAAI Conference on Artificial Intelligence*, volume 33, pages 9299–9306, 2019. [2](#)
- [76] Yang Zhou, Xintong Han, Eli Shechtman, Jose Echevarria, Evangelos Kalogerakis, and Dingzeyu Li. Makelttalk: Speaker-aware talking-head animation. *ACM Trans. Graph.*, 39(6), Nov. 2020. [1](#), [2](#), [5](#), [7](#), [8](#)
- [77] Jun-Yan Zhu, Taesung Park, Phillip Isola, and Alexei A Efros. Unpaired image-to-image translation using cycle-consistent adversarial networks. In *Proceedings of the IEEE international conference on computer vision*, pages 2223–2232, 2017. [2](#)

# Supplemental Document

## AudioViewer: Learning to Visualize Sounds

This document provides details about content and style disentanglement, an additional analysis and details on the user study and training, supplementing the main document. We also prepared an additional supplemental HTML file *index.html* that contains audio and video snippets that can not be played in a conventional PDF. These give additional qualitative results for spoken sentences and environment sounds.

**Licenses:** The used audio datasets TIMIT dataset [1] and ESC-50 dataset [3] in our experiments are public. TIMIT dataset [1] is under the terms of LDC User Agreement for Non-Members license and ESC-50 dataset [3] is under the terms of the Creative Commons Attribution Non-Commercial license.

### 1. Results on Environment Sounds

With the style disentangling training of our AudioViewer method, the audio model is more specific to human speech than general sounds. In the following, we test the generalization capability of our method (trained on the speech TIMIT dataset [1]) on the ESC-50 environment sound dataset [3].

Table 1 shows the reconstruction accuracy when going via the audio and video VAEs (see Information Throughput section in the main document). The SNR for reconstructed Mel spectrum is generally lower than the speech dataset, which is expected since it was trained on the latter. The analysis of the reconstruction ability of the audio VAE in isolation (without going through the video VAE) reported in

Table 1. **Information throughput on environment sounds**, showing that the reconstruction error increases when evaluating on a test set that contains sounds vastly different from the training set (speech vs. environment sounds).

Audio models	Visual models	SNR(dB)
Audio PCA	Visual PCA	17.23
SpeechVAE	DFC-VAE on CelebA	1.03
	DFC-VAE on MNIST	2.22
	DFC-VAE on CelebA (refined w/ $\mathcal{L}_{cycle}$ )	<b>2.83</b>
	DFC-VAE on MNIST (refined w/ $\mathcal{L}_{cycle}$ )	0.76
SpeechVAE w/ $\mathcal{L}_{p,log MSE}$ , $\mathcal{L}_{rr}$ , dim=256	DFC-VAE on CelebA	0.46
	DFC-VAE on MNIST	0.46
	DFC-VAE on CelebA (refined w/ $\mathcal{L}_{cycle}$ )	1.26
	DFC-VAE on MNIST (refined w/ $\mathcal{L}_{cycle}$ )	<b>1.68</b>

Table 2 shows that a large fraction of this loss of accuracy stems from the learning of speech specific features of the audio VAE. Moreover, with a recombined reconstruction loss term on the human speech dataset, the model was fitted to speech features and tended to loss high pitch information. Still, according to the face visualization of the content encoding as we showed in the HTML file, our AudioViewer can generate consistent visualization to given environment sounds.

### 2. Disentangling content and style

We construct a SpeechVAE that disentangles the style (speaker identity) content (phonemes) in the latent encodings, i.e., the latent encoding  $\mathbf{z} = [z_1, \dots, z_d]^T \in \mathcal{R}^d$  can be separated as a style part  $\mathbf{z}_s = [z_1, \dots, z_m]^T$  and a content part  $\mathbf{z}_c = [z_{m+1}, \dots, z_d]^T$ , where  $d$  is the whole audio latent space dimension and  $m$  in the audio style latent space dimension.

We use an audio dataset with phone and speaker ID annotation. However, this still requires to disentangle the audio signal into style and content codes, which we obtain similarly to [4] by mixing embeddings from different speakers. Figure 1 gives an overview. At training time, we feed triplets of mel spectrogram segments  $\mathbf{T}_{a,b,i,j} = \{\mathbf{M}_{a,i}, \mathbf{M}_{b,i}, \mathbf{M}_{a,j}\}$ , where  $\mathbf{M}_{a,i}$  and  $\mathbf{M}_{b,i}$  are the same phoneme sequence  $p_i$  spoken by different speakers  $s_a$  and  $s_b$  respectively, and  $\mathbf{M}_{a,j}$  shares the speaker  $s_a$  with the first segment but a

Table 2. **Audio VAE Mel spectrum reconstruction**. The average SNR of autoencoding and decoding Mel spectrograms on ESC-50 shows a significant reconstruction loss. The average speed and acceleration between the latent vector (dim = 128) of neighbouring frames ( $\Delta t = 0.04s$ ) confirms the experiments in the main document, that smoothness comes at the cost of lower reconstruction accuracy.

Audio models	SNR (dB)	Velocity ( $s^{-1}$ )	Acc. ( $s^{-2}$ )
Audio PCA	<b>17.23</b>	<b>170.13</b>	<b>6960.80</b>
SpeechVAE [2]	10.17	172.57	7331.77
SpeechVAE w/ $\mathcal{L}_{p,log MSE}$	<b>8.92</b>	58.78	1859.95
SpeechVAE w/ $\mathcal{L}_{rr}$	2.98	40.54	1580.86
SpeechVAE w/ $\mathcal{L}_{p,log MSE}, \mathcal{L}_{rr}$	2.19	<b>30.66</b>	<b>909.39</b>
SpeechVAE w/ $\mathcal{L}_{p,log MSE}, \mathcal{L}_{rr}$ , dim=256	2.51	33.88	1037.97



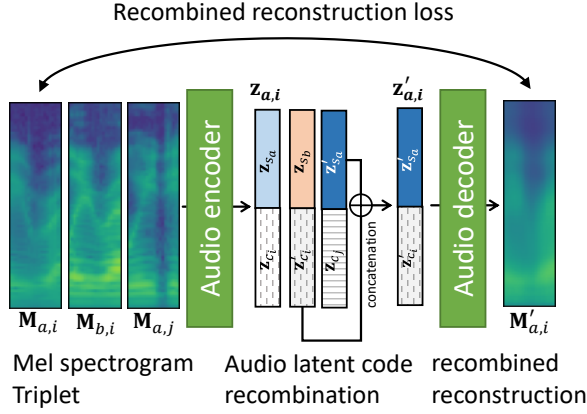


Figure 1. **Disentanglement**, by mixing content encodings from two speakers saying the same phones ( $z_{c_i}$  with  $z'_{c_i}$ ) and style encodings from the same speaker saying different words ( $z_{s_a}$  with  $z'_{s_a}$ ).

different phoneme sequence. Each element of the input triplet is encoded individually by  $E_A$ , forming latent triplet  $\{z_{a,i}, z_{b,i}, z_{a,j}\} = \{[z_{s_a}, z_{c_i}]^T, [z_{s_b}, z'_{c_i}]^T, [z'_{s_a}, z_{c_j}]^T\}$ , instead of reconstructing the inputs from the corresponding latent encodings in an autoencoder, we reconstructed the first sample  $M_{a,i}$  from a recombined latent encoding of the other two,  $z'_{a,i} = [z'_{s_a}, z'_{c_i}]^T$ . Formally, we replaced the reconstruction loss term in the VAE objective by a recombined reconstruction loss term,

$$\mathcal{L}_{rr}(\mathbf{T}_{a,b,i,j}) = \mathbb{E}_{q_\phi(z'_{a,i} | M_{b,i}, M_{a,j})} (\log p_\theta(M_{a,i} | z'_{a,i})). \quad (1)$$

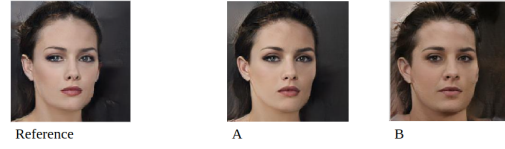
This setup forces the model to learn separate encodings for the style and phoneme information while not requiring additional loss terms.

Note that we could alternatively enforce  $z_{a,i}$  to be close to  $z'_{a,i}$  without decoding (the unused  $z_{a,i}$  in Figure 1). However, an additional L2 loss on the latent space led to a bias towards zero and lower reconstruction scores than the proposed mixing strategy that works with the original VAE objective.

### 3. User Study I - Discriminating Sounds

Our user study I required participants to complete one of 5 versions of a questionnaire: disentangled content model with CelebA-HQ visualizations (CelebA-HQ-content), disentangled content model with CelebA visualizations (CelebA-content), disentangled style model with CelebA visualizations (CelebA-style), disentangled content model with MNIST visualizations (MNIST-content) and a combined model with CelebA visualizations (CelebA-combined). Each version of the questionnaire asked the same set of 29 questions with randomized ordering of answers within each question. The study was conducted with 22, 14, 15, 12, 14, and 14 participants for the CelebA-HQ-content, CelebA-content, CelebA-style, CelebA-combined, MNIST-content,

#### Question 11



Indicate the above image (A or B) that is most similar to the reference image:

☐ A ☐ B

#### Question 11



Indicate the above image (A or B) that is most similar to the reference image:

☐ A ☐ B

#### Question 11



Indicate the above image (A or B) that is most similar to the reference image:

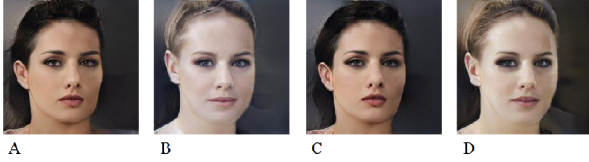
☐ A ☐ B

Figure 2. **Matching Example.** Examples from the CelebA-HQ-content, CelebA-combined and MNIST-content questionnaire of a matching question asked to participants in the user study.

and MakeItTalk [5] questionnaires, respectively. Amongst all the questionnaires that evaluate AudioViewer, there were 45 unique participants. In addition, 14 participants completed the MakeItTalk [5] questionnaire. It took participants between 10-15 minutes to complete the each questionnaire. The questionnaire asked participant to perform two possible tasks: matching and grouping visualizations. The format of the questionnaire is outlined in Table 3. The questions tested for two factors: sound content, sounds that share the same phoneme sequences, and sound style, sounds produced by speakers of the same sex or speaker dialect. This purely visual comparison allows us analyze different aspects of the translation task individually.

**Matching questions** Matching questions asked the participants to choose which of two possible visualizations which is most visually similar to a given reference visual. Figure 2 shows examples of matching questions. Matching questions were used to assess the viability for users to distinguish between the same sounds produced by speakers

#### Question 23



Group the above images (A - D) into pairs of similar images:

☐ AB, CD ☐ AC, BD ☐ AD, BC

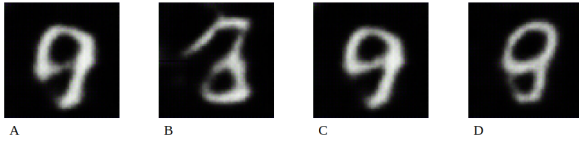
#### Question 23



Group the above images (A - D) into pairs of similar images:

☐ AB, CD ☐ AC, BD ☐ AD, BC

#### Question 23



Group the above images (A - D) into pairs of similar images:

☐ AB, CD ☐ AC, BD ☐ AD, BC

Figure 3. **Grouping Example.** Examples from the CelebA-HQ-content, CelebA-combined and MNIST-content questionnaire of a grouping question asked to participants in the user study.

Table 3. **A breakdown of the questionnaire format** by sound type and tested factors, listing their frequency of occurrence.

Question type	Sound type	Tested factor	Questions
Matching questions	Phone-pairs	Content	3
		Style (sex)	3
		Style (dialect)	2
	Words	Content	3
		Style (sex)	3
		Style (dialect)	2
Grouping questions	Phone-pairs	Content + style (dialect)	2
		Content + style (dialect + sex)	2
	Words	Content	3
		Content + style (dialect)	2
		Content + style (sex)	1
		Content + style (dialect + sex)	1
		Content (similar sounding words)	2
Total			29

possessing different speaker traits as well as determining whether structural similarities in the underlying audio translated into similarities in the visualization. In particular, the questionnaire contained 6 questions for evaluating the abil-

Table 4. **User study results.** Values indicate mean accuracy and standard deviation for distinguishing between visualizations of the tested factor across participants as a percentage. The disentangled representation clearly outperforms the combined baseline.

Tested Factor	PCA-Baseline	CelebA-disentangled	CelebA-combined
Content	38.4	<b>85.0 <math>\pm</math> 6.8</b>	72.8 $\pm$ 10.0
Style (dialect)	50.0	<b>56.7 <math>\pm</math> 22.1</b>	39.6 $\pm$ 24.9
Style (sex)	43.3	<b>78.0 <math>\pm</math> 10.8</b>	43.3 $\pm$ 8.9

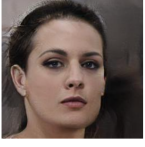
ity to distinguish between sound content, which compared visualizations of sounds of different phoneme sequences (3 for phoneme-pairs and 3 for words). Phone-pairs are short in length and therefore the corresponding visualisation was a single frame image, whereas visualisations of words were videos. In order to evaluate the ability to distinguish between sound style, 6 questions compared visualizations of the same phoneme sequence between male and female speakers and 4 questions for distinguishing between speakers of different dialects. In total there were 16 matching questions. Since each question has two options, the expected mean accuracy for random guessing is 50%.

**Grouping questions** Grouping questions asked the participants to group 4 visualizations into two pairs of similar visualizations. Figure 3 shows examples of grouping questions. Grouping questions were used to assess the degree to which visualizations of different words are distinguishable and visualizations of the same word are similar. In particular, the study required users to group visualizations of two pairs of sounds, whereby different pairs are sound clips with shared factors of the same sound content or same sound style. In total, the user study consisted of 4 grouping questions based on phone-pairs and 9 grouping questions based on words. Since there are three possible options, the expected mean accuracy for random guessing is 33.3%.

**Results** For each of the models, we tested for sound content: phoneme sequences, and sound style: speaker dialect and speaker sound. We generated the mean accuracy and standard deviation for each tested factor and each question sub type. Table 4 extends the results shown in the main document by comparing entangled and disentangled representations. The results of the disentangled models with CelebA visualizations (CelebA-disentangled) is aggregated by taking the results of CelebA-content on the questions which tested for sound content and the results of CelebA-style on questions which tested for sound style.

Figure 6 shows users achieve the highest overall accuracy on the CelebA-disentangled model with  $85.0 \pm 6.8\%$  (significant with  $p < 0.05$ ) for distinguishing between visualizations of different content. The MNIST-content model has the highest accuracy for distinguishing between different phone pairs with  $91.8 \pm 9.2\%$ , although not sig-

**Instructions:** You will be shown visualizations of sounds. After how many trials will you be able to recognize a sound by its visualization?

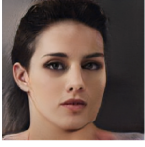


**Example 1:** Please select the sound that is visualized above

Sound k | Sound k\_s | Sound tcl | Sound d\_aa

You will receive feedback after every answer and improve over time.

**Instructions:** You will be shown visualizations of sounds. After how many trials will you be able to recognize a sound by its visualization?



**Example 1:** Please select the sound that is visualized above

Replay ▶ | Sound potatoes | Sound shellfish | Sound that | Sound there

You will receive feedback after every answer and improve over time.

Figure 4. **Learning sounds examples.** A video generated by the disentangled content model is shown to evaluate the participants' capability in learning to recognize sounds from visual contexts. Each video corresponds to one variant of four phone/word labels.

nificantly higher than the CelebA-disentangled one with ( $p > 0.05$ ), but has a much lower accuracy for distinguishing between different words, suggesting that the MNIST visualizations may be better suited for representing shorter sounds. The CelebA-disentangled model outperforms the CelebA-combined model for distinguishing between speakers of different sex with  $78.0 \pm 10.8\%$  (significant with  $p < 0.001$ ) and between speakers of different dialects with  $56.7 \pm 22.1\%$  (marginally significant with  $0.05 < p < 0.10$ ) as shown in Figure 7. The task of distinguishing between different speakers of different dialects is much more difficult than distinguishing between phoneme sequences since there are 8 categories of dialects in the dataset and differences in dialects are much more subtle and can contain often contain overlaps. Significance comparing model means were calculated using a two-sample two-tailed t-test with unequal variance and without any outlier rejection.

#### 4. User Study II - Learning Sounds

In the second study, we evaluate whether participants can learn to recognize sounds from our visualizations. Specif-

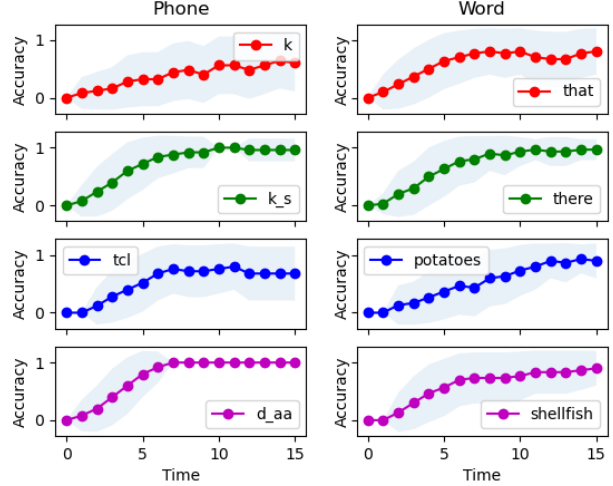


Figure 5. **Learning curve.** Participants learn over time to recognize phones (left) and words (right). Accuracy is plotted as the moving average of the success rate over trials.

ically, five participants are asked to complete two iterative learning processes independently, one for phone learning and the other for word learning, with a group of phone samples and another group of word samples. The phone samples include two phones with similar pronunciation, *k* and *k\_s*, and two differentiated samples, *tcl* and *d\_aa*. Similarly, the word samples include two words with similar pronunciation, 'that' and 'there', and two samples with large differences, 'potatoes' and 'shellfish'. These sound samples come from speakers of the same gender but in different dialects. For each sound, we show six different variations and for each word, we show four. This totals to 24 sound visualizations and 16 word visualizations. The corresponding videos are from the visual results transferred by the disentangled content model with the high-res CelebA-HQ. Examples of user learning are shown in Figure 4. For phone/word learning, we randomly select a transferred video. The participants are required to choose the corresponding phone/word label, and then the correct result will be disclosed in the form of feedback. The perceptibility of our method is evaluated by tracking the changes in the accuracy curves.

**Results** It took participants between 10-15 minutes to complete each variant. Figure 5 illustrates the average learning accuracy curve of all participants. Values are averaged over five frames to compute non-binary accuracy numbers for every individual participant. The light blue bands represent the standard deviation across different subjects. The final recognition accuracy of most phones and words reaches close to 100% and even the similar sounds, like *k* and *k\_s*, 'that' and 'there', can also be well distinguished, which demonstrates the learnability.

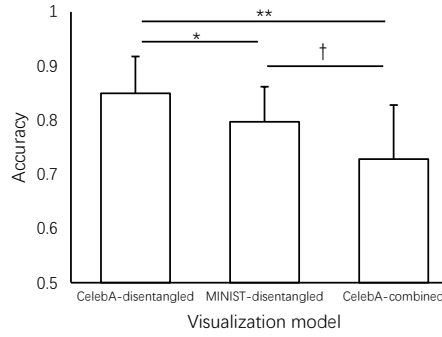


Figure 6. **Model Comparison on content questions.** The mean user accuracy and standard deviation for distinguishing phoneme sequences is compared between the models, annotated with the significance level ( $\dagger$  for  $0.05 < p < 0.1$ ,  $*$  for  $p < 0.05$ ,  $**$  for  $p < 0.01$ ). The mean accuracy for random guessing is 0.384.

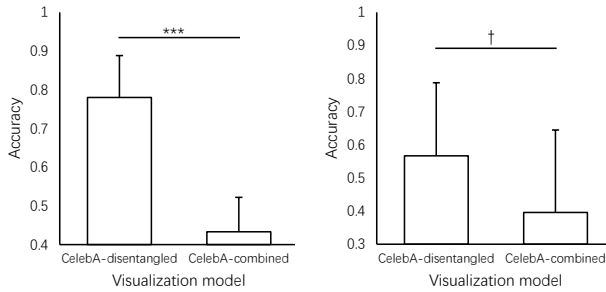


Figure 7. **Model Comparison on style questions.** The mean user accuracy and standard deviation for distinguishing speaker sex (left) and dialect(right) is compared between the models, annotated with the significance level ( $\dagger$  for  $0.05 < p < 0.1$ ,  $***$  for  $p < 0.001$ ). The mean accuracies for random guessing are 0.43 and 0.5 respectively.

## References

- [1] John S Garofolo. Timit acoustic phonetic continuous speech corpus. *Linguistic Data Consortium, 1993*, 1993. [1](#)
- [2] Wei-Ning Hsu, Yu Zhang, and James Glass. Learning latent representations for speech generation and transformation. In *Interspeech*, pages 1273–1277, 2017. [1](#)
- [3] Karol J Piczak. Esc: Dataset for environmental sound classification. In *Proceedings of the 23rd ACM international conference on Multimedia*, pages 1015–1018, 2015. [1](#)
- [4] Kaizhi Qian, Yang Zhang, Shiyu Chang, Xuesong Yang, and Mark Hasegawa-Johnson. Autovc: Zero-shot voice style transfer with only autoencoder loss. In *International Conference on Machine Learning*, pages 5210–5219. PMLR, 2019. [1](#)
- [5] Yang Zhou, Xintong Han, Eli Shechtman, Jose Echevarria, Evangelos Kalogerakis, and Dingzeyu Li. Makeltalk: Speaker-aware talking-head animation. *ACM Trans. Graph.*, 39(6), Nov. 2020. [2](#)